Empowering Off-Road Diesel Powertrains: Advanced Multivariate Air Handling Control for Electrified Performance

Shubham Ashta, Nicholas Vang, Weijin Qiu, Chisom Emegoakor, Sree Harsha Rayasam, Tyler Swedes, Jacob Mazanec, Giraldo Luis, Bryan Frushour, Gregory Shaver, Sage Kokjohn, Jaal Ghandhi and David Rothamer

Abstract

This conference paper delves into the advantages of employing an electrified intake boosting system in a 4.5L John Deere diesel engine. The electrified intake system (eBooster) strategically activates solely during transient operations to mitigate drops in the air-to-fuel ratio (AFR) that may result in smoke emissions. To adeptly oversee the electrified air handling system, we introduce a two-degree-of-freedom robust H_∞ single-input single-output (SISO) eBooster controller and a robust model-based H_∞ multiple-input multiple-output (MIMO) controller. These controllers are engineered to regulate the desired AFR, engine speed, and diluent air ratio (DAR) through the manipulation of various air handling actuators (exhaust throttle and EGR valve) and fueling strategies.

The robust SISO controller is crafted utilizing a linear plant model derived through system identification, while the robust MIMO controller is developed based on a physics-based mean value engine model meticulously calibrated to accurately replicate high-fidelity engine simulation software. Both controllers are subjected to simulation using high-fidelity engine simulation software, followed by validation through experimental testing on an engine dynamometer at the University of Wisconsin. Results are benchmarked against a non-eBoosted engine, serving as the baseline. While both the SISO and MIMO controllers exhibit improvements in AFR, DAR, and engine speed recovery during load transients, the robust MIMO controller outperforms them, showcasing superior overall engine performance. This superiority is attributed to its nuanced understanding of the coupling between each actuator input and the model output.

Operating in tandem with the electrified intake boosting system, the MIMO controller brings about significant enhancements. The engine not only recovers to a steady state 70% faster than the baseline but also mitigates engine speed droop by 45%. Consequently, the engine's ability to accommodate load torque sees a substantial increase, underscoring the benefits of an electrified air handling system governed by a robust MIMO controller.

Keywords. Heavy Duty Diesel Engine Operation, Robust Multivariate Control, Electrified Air Handling System

1. INTRODUCTION

Diesel engines have gained extensive traction in heavy-duty off-road applications owing to their robust torque output, durability, and fuel efficiency [1]. These engines demonstrate remarkable performance in tasks demanding substantial power and resilience in harsh environments. Recognizing the substantial emissions associated with diesel engines [2], prioritizing fuel efficiency emerges as a pivotal consideration in the development of heavy-duty diesel powertrains.

In response to stringent emission regulations and fuel economy objectives, engine downsizing utilizing turbomachinery has emerged as a prevalent strategy to meet these imperatives. Downsizing facilitates reduced fuel consumption while upholding equivalent power and torque compared to non-downsized engines. Moreover, downsized engines typically exhibit reduced weight, contributing to overall vehicle weight reduction. This reduction translates into diminished energy requirements for acceleration and maintaining velocity, thereby yielding noteworthy fuel savings.

Moreover, under part load operating conditions, downsized engines offer the potential to enhance fuel efficiency [3]. Turbochargers frequently feature in downsized diesel engines, enhancing fuel efficiency, bolstering low-end torque, and mitigating emissions [20].

Boosting technologies are pivotal in facilitating engine downsizing, thereby enhancing thermal efficiency and brake mean effective pressure (BMEP) [4]. In pursuit of further enhancing the capabilities of these downsized powertrains, electrified boosting technologies emerge as a promising solution [5]. Electrified intake boosting systems provide immediate boost pressure, eliminating the typical turbo lag associated with conventional mechanical turbochargers. This instantaneous boost substantially improves engine responsiveness, particularly during transient load operations, by minimizing air-fuel ratio (AFR) recovery delays.

Integrating electrified boosting systems into hybridized powertrains represents a significant advancement in enhancing fuel efficiency. By harnessing energy from regenerative braking and repurposing wasted engine exhaust gas, this integration optimizes fuel conservation [6][7][8]. Previous endeavors, including those detailed by Nazari [9][10], underscore the significance of decentralized control schemes in air handling systems featuring electrified boosting, with a focus on diminishing turbo lag to enhance engine speed response. Moreover, innovations like frequency separation controllers [11], SISO AFR controllers for electric turbochargers [12], and SISO AFR controllers for downsized gasoline engines [13] contribute to the dynamic landscape of engine control strategies. Nonetheless, the intricate and nonlinear characteristics of air handling systems in diesel engines, incorporating various actuators like exhaust throttles and EGR valves, pose challenges. These systems often exhibit MIMO characteristics, emphasizing the complex interplay between actuators and outputs.

The Relative Gain Array (RGA) analysis offers a method for assessing the degree of Multiple Input Multiple Output (MIMO) coupling in a system [14]. In the study conducted by Harsha et al. [15], the focus lies on developing such a MIMO system and analyzing various couplings using RGA analysis. Despite the benefits of decentralized controllers for MIMO systems, the overall engine performance might still fall short of optimal. This situation calls for exploring multivariate control strategies to effectively handle such intricate air handling systems. An example of such an approach is demonstrated in the work highlighted in [16] and [18], where a robust multivariate controller is devised for a turbocharged natural gas engine and switching algorithms are developed to use multiple controllers at different operating points [17][19].

Addressing the requirement for downsized, e-boosted, power-dense Internal Combustion (IC) engines used in demanding commercial vehicle applications, this paper discusses the creation and deployment of robust Single Input Single Output (SISO) and MIMO H_∞ feedback controllers for a heavy-duty diesel powertrain equipped with an electrically driven intake boosting system for a downsized 4.5L John Deere diesel engine. The electrified compressor (eBooster) from BorgWarner is selected for implementation on the downsized diesel engine. These controllers aim at managing multiple outputs: engine speed for torque/power regulation, air-fuel ratio (AFR) for controlling smoke emissions, and diluent air ratio (DAR) to regulate engine NOx emissions. H_∞ controller tuning is iterative and it requires a certain methodology to get the optimal results [21].

The initial emphasis of this research is on the robust SISO eBooster controller, which aims to maintain the desired AFR by specifically controlling the eBooster speed during load changes. Subsequently, a robust MIMO eBooster controller is developed. A nonlinear state space mean value model is constructed to represent the engine's air handling system, which is validated against engine simulations. This nonlinear model is then linearized for robust MIMO controller synthesis.

To showcase the effectiveness of these control strategies, the SISO and MIMO controllers are experimentally verified on the engine coupled to a dynamometer, and their performance is compared against the baseline non-eBoosted engine, illustrating the benefits of multivariate control strategies for air handling systems.

2. ROBUST SISO EBOOSTER CONTROL DEVELOPMENT

The initial phase in the development of an eBooster controller involved synthesizing a SISO H_∞ feedback controller. Implementing this controller is comparatively simpler than integrating the MIMO controller with the stock ECM (Engine Control Module). The SISO eBooster controller aims to recover the Air-Fuel Ratio (AFR) by adjusting eBooster speed during transients, while the ECM manages the remaining aspects of the engine's air handling system.

2.1. Controller Configuration

The primary objective of the robust SISO controller is to restore the engine's Air-Fuel Ratio (AFR) during transient load operations. As engine load increases, the fueling commanded by the ECM rises to generate more brake torque, thereby maintaining engine speed. However, this increased fueling can lead to a temporary dip in the engine's AFR, potentially resulting in unwanted smoke emissions. By introducing additional air through an electrically driven intake boosting system, the AFR can be restored more rapidly during transient operations.

Figure 2.1 illustrates the configuration of the controller utilized to synthesize the SISO eBooster controller. This configuration entails a 2-degree of freedom controller with inputs consisting of Desired and Measured AFR, while the controller output dictates the commanded eBooster speed. Multiplicative uncertainty for the output was incorporated during controller synthesis. The Desired AFR serves as the exogenous input to the system, while the weighted AFR and weighted eBooster Speed serve as the exogenous outputs.

Further elucidation on the controller configuration will be provided in the subsequent discussion on the Development of Robust MIMO eBooster Controller.

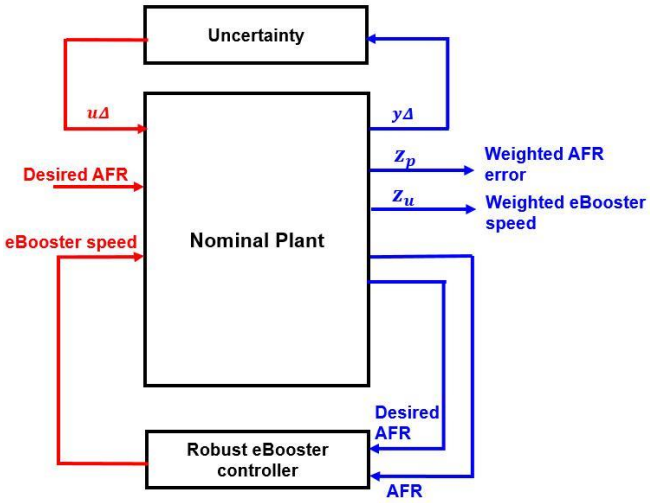

Figure 2.1. Controller Configuration for SISO eBooster controller

2.1.1. System Identification for Plant Model Development

A nominal plant model is derived via the system identification process to relate the effect of eBooster speed on the AFR of the engine. The relationship is defined as

$$G(s) = \frac{Y(s)}{U(s)} \tag{2.1}$$

where G(s) represent the transfer function for the plant model, Y(s) is the plant output representing the engine's AFR response and U(s) is the plant input representing the commanded eBooster speed. For system identification of the plant model, we utilize the 4.5L single turbo engine housed in the engine test cell as a truth reference (Fig. 2.2). The engine operates in closed-loop control mode at the desired torque and speed within the test cell. Once a steady state is attained, a step change in the eBooster speed is commanded to transition from 2000 rpm to 50000 rpm (with the eBooster's maximum speed capped at 70000 rpm) for the system identification procedure. The engine's Air-Fuel Ratio (AFR) response is logged via dSPACE, employing a wideband lambda sensor to discern the plant dynamics accurately. This process is iterated across various operating points of the engine for comprehensive analysis and model estimation.

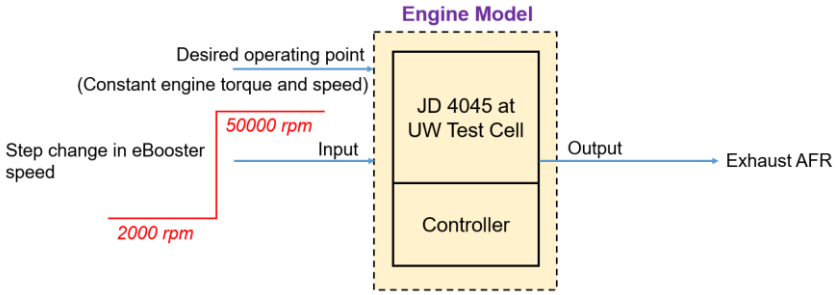

Figure 2.2. System Identification Process

The AFR responses of the engine indicate that a first-order plant transfer function ($G(s) = \frac{K}{(\tau s+1)}$) serves as a suitable approximation for illustrating the engine's dynamics across different load and speed points.

2.2. Plant Uncertainty Weight

Several plant models were developed using the system identification process above in order to estimate the plant dynamics of the engine. Using these transfer functions, a nominal plant model is estimated:

$$G(s) = \frac{7.61 \times 10^{-4}}{(0.4627s + 1)} \tag{2.2}$$

The nominal plant model developed loses accuracy at different operating points. To account for this uncertainty the plant model output, a multiplicative uncertainty weight is defined as a frequency dependent weight.

$$w_i = \frac{(0.25s + 0.35)}{(0.45s + 1)} \tag{2.3}$$

Figure 2.4 shows various samples of possible relative uncertainties and w_i chosen to be greater than these relative uncertainties.

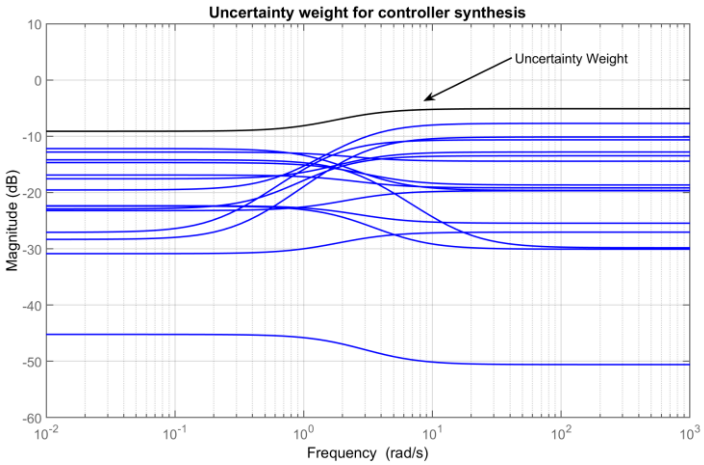

Figure 2.4. Plant Model Uncertainties

2.3. Performance and Actuator Weighting Functions

The performance (W_p) and actuator weighting (W_u) functions are designed to control shape the AFR error and penalize control usage respectively. The performance weighting function provides the upper bound to the complimentary transfer function of the system while actuator weighting function helps provide physical limitations to the commanded eBooster speed.

To shape the AFR error, the performance weighting function in frequency domain is defined as

$$W_p = \left(\frac{\frac{s}{M} + \omega_B}{s + \omega_B A} \right) \tag{2.4}$$

where M represents max error at high frequency, A represents the steady state error in AFR, ω_B represents the frequency at which the error is 100%.

The tuned values for the above parameters are shown below.

$$M = 8 \quad A = 0.7 \quad \omega_B = 4 \frac{rad}{s}$$

Similarly, the actuator weighting function is defined as

$$W_u = \left(\frac{\frac{s}{3.7} + 1}{\frac{s}{370} + 1} \right) \tag{2.5}$$

Figure 2.5 shows the bode magnitude plots of the inverse performance weight $W_P^{-1}$and inverse actuator weight W_u^{-1}.

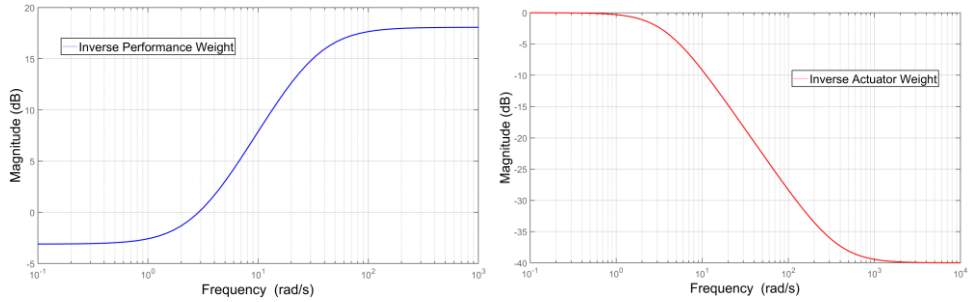

Figure 2.5. Inverse Performance and Actual Weighting Functions

Although SISO eBooster control showcases the benefits of eBoosting during load transient operation, the air handling system is also affected by other actuators in the system (EGR and Exhaust throttle valve). There is a need to develop a robust multiple input multiple output (MIMO) controller that can handle all the actuators while being able to the track the desired reference targets. The following section discusses the development of a robust MIMO controller.

3. ROBUST MIMO CONTROL DEVELOPMENT

A robust multiple input multiple output controller is hypothesized to provide the most optimal control action for the electrified air handling system of the downsized diesel engine as shown in the figure 3.1. To develop such a controller, a non-linear state space (NLSS) representation is developed to model the dynamics of various actuators and their effect on various outputs. The NLSS model is described in the figure 3.2 with various states that affect the air handling system of the diesel engine.

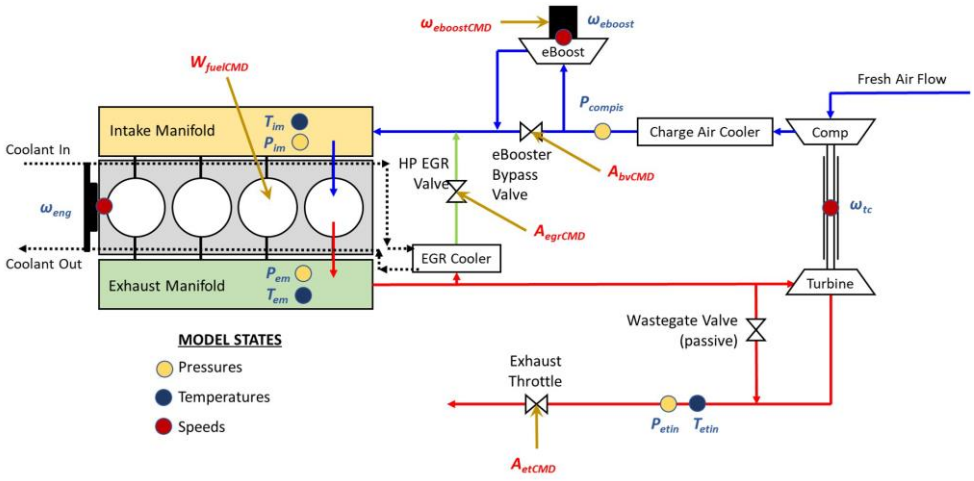

Figure 3.1. Electrified Air Handling System Architecture

3.1. NLSS Model Development

These NLSS model states are described using the following equations.

$$\dot{x} = f(x, u, u_d)$$

$$y = g(x, u)$$

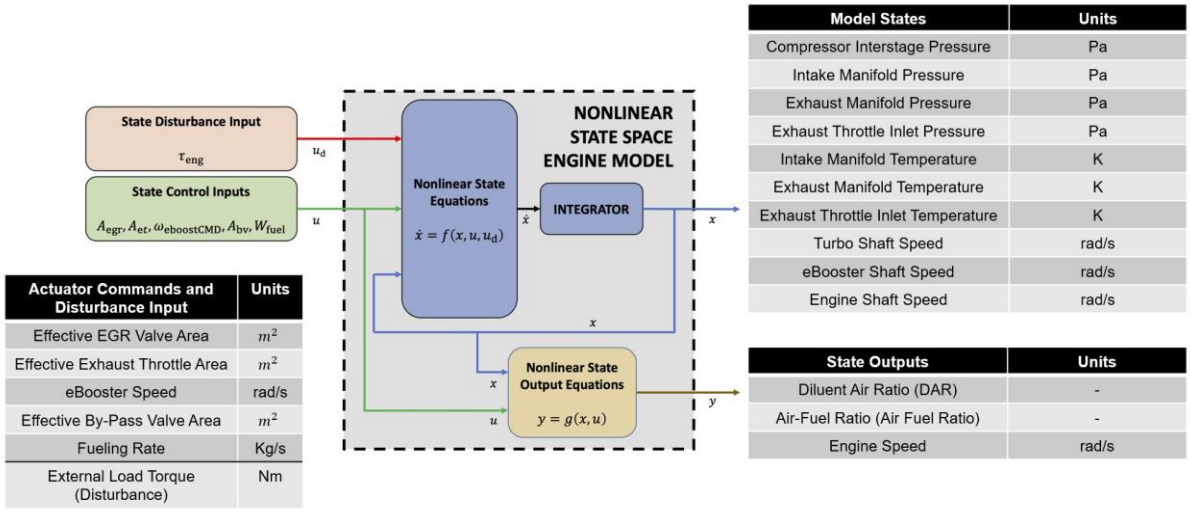

Figure 3.2. NLSS Model Representation

Where x represents the model states, u represents the actuator inputs, u_d represents the disturbance input (load torque) and y represents the state outputs.

The ten model states and the model outputs are governed by the dynamic equations as shown in figure 3.3. The pressure and temperature states are derived by conducting a thermodynamic analysis for various manifolds. Torque analysis around the crankshaft and turbocharger shaft is used to estimate the dynamics of the speed states. While some variables are considered as constants (e.g. manifold volumes, inertias), others are represented as internal sub models based upon various model states and inputs (as shown in figure 3.3). These sub models are derived as parameterized curve fits using the high-fidelity engine simulation software as truth reference.

The tuned high-fidelity model is used as a truth reference for the non-linear model validation process. This is an open loop validation and is represented in figure 3.4. The desired engine speed and load torque are simulated in GT Power (running with various internal controllers). The actuator commands generated from the controllers are used as actuator inputs to the non-linear state space model.

Dynamic Equations (Model States)

$$\dot{x}_1 = P_{\dot{compis}} = \frac{\gamma_{amb} R}{V_{compis}} \left[W_{comp} T_{CAC} + W_{eBoost} T_{CAC} - W_{bv} T_{CAC} \right]$$

$$\dot{x}_2 = P_{\dot{im}} = \frac{\gamma_{im} R}{V_{im}} \left[W_{egr} T_{egr} + W_{eBoost} T_{eBoost,out} + W_{bv} T_{CAC} - W_{cyl} T_{im} \right]$$

$$\dot{x}_3 = P_{\dot{em}} = \frac{\gamma_{ex} R}{V_{em}} \left[W_{cylout} T_{cylout} - W_{turb} T_{em} - W_{wg} T_{em} - W_{egr} T_{em} \right]$$

$$\dot{x}_4 = P_{\dot{etin}} = \frac{\gamma_{ex} R}{V_{etin}} \left[W_{wg} T_{em} + W_{turb} T_{turb,out} - W_{et} T_{etin} \right]$$

$$\dot{x}_5 = T_{\dot{im}} = \frac{R_{im} T_{im}}{P_{im} V_{im}} \left[W_{eBoost} \left(\gamma_{amb} T_{eBoost,out} - T_{im} \right) + W_{egr} \left(\gamma_{ex} T_{egr} - T_{im} \right) + W_{bv} \left(\gamma_{amb} T_{CAC} - T_{im} \right) - W_{cyl} \left(\gamma_{im} T_{im} - T_{im} \right) \right]$$

$$\dot{x}_6 = T_{\dot{em}} = \frac{R_{em} T_{em}}{P_{em} V_{em}} \left[W_{cylout} \left(\gamma_{cylout} T_{cylout} - T_{em} \right) - \left(W_{turb} + W_{wg} + W_{egr} \right) \left(\gamma_{ex} T_{em} - T_{em} \right) \right]$$

$$\dot{x}_7 = T_{\dot{etin}} = \frac{R_{etin} T_{etin}}{P_{etin} V_{etin}} \left[W_{wg} \left(\gamma_{ex} T_{em} - T_{etin} \right) + W_{turb} \left(\gamma_{ex} T_{turb,out} - T_{etin} \right) - W_{et} \left(\gamma_{ex} T_{etin} - T_{etin} \right) \right]$$

$$\dot{x}_8 = \omega_{\dot{tc}} = \frac{Z_{turb} - Z_{comp}}{I_{tc} \omega_{tc}}$$

$$\dot{x}_9 = \omega_{\dot{eBoost}} = \frac{\omega_{eBoostCMD} - \omega_{eBoost}}{\tau_{eBoost}}$$

$$\dot{x}_{10} = \omega_{\dot{eng}} = \frac{C_{trq} P_{im} - \tau_{eng}}{I_{eng}}$$

Summary of Submodels Used

Parameter	Description	Submodel
W_{eBoost}	eBooster Compressor Flow	$fcn(x_1, x_2)$
W_{comp}	Turbocharger Compressor Flow	$fcn(x_1)$
W_{bv}	eBooster Bypass Flow	$fcn(x_1, x_2, u_4)$
W_{cyl}	Cylinder-In Flow Rate	$fcn(x_2, x_5, x_{10})$
W_{egr}	EGR Flow Rate	$fcn(x_2, x_3, u_1)$
W_{turb}	Turbine Flow Rate	$fcn(x_3, x_4, x_6)$
W_{et}	Exhaust Throttle Flow Rate	$fcn(x_4, x_7, u_2)$
Z_{comp}	Compressor Power	$fcn(x_1, x_8)$
Z_{turb}	Turbine Power	$fcn(x_3, x_4, x_6, x_8)$
$T_{eBoost,out}$	eBooster Outlet Temperature	$fcn(x_1, x_2)$
T_{cylout}	Cylinder Outlet Temperature	$fcn(x_2, x_3, x_5, x_{10}, u_5)$
C_{trq}	Engine Torque Coefficient	$fcn(x_1, x_5, x_{10}, u_5)$

Dynamic Equations (Model Outputs)

$$y_1 = DAR = \frac{(AFR_{stoich} + 1) W_{fuel}}{W_{fuel} + W_{comp}} \cdot \left(\frac{W_{egr} + W_{res}}{W_{egr} + W_{res} + W_{comp} - \frac{(AFR_{stoich}+1)(W_{fuel}(W_{egr}+W_{res}))}{W_{fuel}+W_{comp}}} \right)$$

$$y_2 = AFR = \frac{W_{comp}}{W_{fuel}}$$

$$y_3 = \omega_{eng} = x_{10}$$

Figure 3.3. Dynamic Equations for the NLSS Model

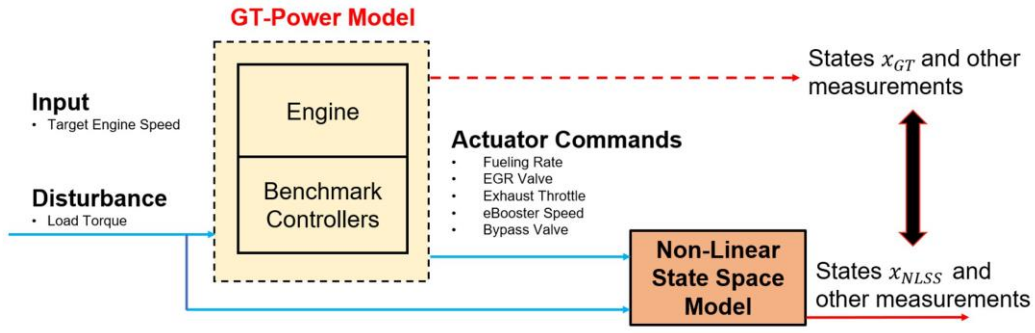

Figure 3.3. NLSS Model Validation

3.2. Model Linearization

The NLSS model is then linearized around the equilibrium of our choice to be used as plant model for controller synthesis. This linearized plant model is represented as:

$$\dot{x} = \delta\dot{x} = A\delta x + B\delta u + F\delta u_d$$

$$\delta y = C\delta x + D\delta u$$

$$\delta x = x - x_e \qquad \delta y = y - y_e \qquad \delta u = u - u_e \qquad \delta u_d = u_d - (u_d)_e$$

Here, x, y, u and u_d are the model state inputs and outputs as discussed in 2.3.3. The variables x_e, u_e, y_e and $(u_d)_e$ represent the equilibrium values around which the non-linear state space model is linearized. The variables δx, δy, δu, and δu_d are the linear model state inputs and outputs. The state space matrices A, B, C, D, and F are estimated by taking the Jacobian of the non-linear differential equations.

The equilibrium values around which the model is linearized, are presented in table 3.1 below.

State/Input	**Parameter**	**Equilibrium Value**	**Units**
x_1	Compressor Interstage Pressure	155.83	kPa
x_2	Intake Manifold Pressure	174.39	kPa
x_3	Exhaust Manifold Pressure	211.61	kPa
x_4	Exhaust Throttle Inlet Pressure	127.62	kPa
x_5	Intake Manifold Temperature	323.37	K
x_6	Exhaust Manifold Temperature	756.95	K
x_7	Exhaust Throttle Inlet Temperature	663.94	K
x_8	Turbo Shaft Speed	85.7	krpm
x_9	eBooster Shaft Speed	45	krpm
x_{10}	Engine Shaft Speed	1800	rpm
u_1	EGR Valve Area	1.07 (24% of max)	m^2
u_2	Exhaust Throttle Area	5.65 (23% of max)	m^2
u_3	eBooster Speed	55000 (78% of max)	rpm
u_4	eBooster By-pass Valve Angle	0 (0% of max)	Degrees
u_5	Total Fueling	3.6	g/s
u_d	Load Torque	300	Nm

Table 3.1 Equilibrium Point for Model Linearization

The equilibrium values are selected to linearize the nonlinear plant model within the midrange of the engine's operating spectrum, where uncertainties will be assigned to account for potential inaccuracies. This engine operates within a hybridized powertrain, maintaining a constant speed of 1800 rpm while handling load torque from both the hydraulic system and the generator used to charge the battery [22]. Accordingly, the equilibrium point was set at 1800 rpm and a load torque of 300 Nm.

3.3. Model Uncertainty Weights

The linearized state space model is used as the nominal plant model for controller synthesis. This nominal model is accurate at the equilibrium point (table 3.1) but loses accuracy at operating points away from its equilibrium. To account for these inaccuracies, multiplicative output uncertainty is assigned to the model outputs as a diagonal matrix. Each element is this matrix is a frequency dependent transfer function and is expressed in the equation below.

$$\delta y = \delta\overline{y_o}\left(1 + W_y\Delta_y\right) \qquad (2.6)$$

Here, $\Delta_y = diag\{y_1, y_2, y_3\}$ and $\delta y_i \in [-1,1]$

$$W_y = \begin{bmatrix} \left(\frac{\frac{s}{20}+1}{\frac{s}{4}+1}\right) & 0 & 0 \\ 0 & \left(\frac{\frac{s}{20}+1}{\frac{s}{4}+1}\right) & 0 \\ 0 & 0 & \left(\frac{\frac{s}{20}+1}{\frac{s}{4}+1}\right) \end{bmatrix}$$

3.4. Performance and Actuator Weighting Functions

The exogenous outputs for various actuators (z_u) and target errors (z_p) are defined using equation 2.7 below.

$$z_u = W_u e \qquad z_p = W_p e \tag{2.7}$$

Where e represents the target error ($y - r$), u represents the actuator command, W_u and W_p represent the actuator and performance weighting functions respectively. To shape the respective errors in frequency domain, the following performance weight (n^{th} order) is used.

$$W_p = K\left(\frac{\frac{s}{M} + \omega_B}{s + \omega_B A}\right)^n \tag{2.8}$$

Where, M represents max error at high frequency, A represents the steady state error in AFR, ω_B represents the frequency at which the error is 100%, n represents the order of the weighting function, K is the scalar multiplied to increase/decrease the weightage to the tracking performance. Table 3.2 below shows the value of each parameter for each of the three outputs (AFR, DAR, Engine Speed) used in simulation as well as on the engine in the engine test cell.

y_i	Implementation in Simulation					Implementation in Engine Test Cell				
	ω_B	M	A	n	K	ω_B	M	A	n	K
DAR	3	0.5	0.001	2	1	8	0.5	0.01	1	1
AFR	1	5	0.1	1	0.5	1	5	0.5	1	0.5
Engine Speed	2.5	0.4	0.01	1	1	2	0.5	0.01	1	4

Table 3.2 Performance Weighting Functions

The actuator weighting function is defined using the equation below.

$$W_u = \frac{1}{N} * \frac{\frac{s}{\left(\frac{\tau}{N}\right)} + 1}{\frac{s}{\left(\frac{\tau}{\epsilon}\right)} + 1} \tag{2.9}$$

Where, N represents control action at low frequencies, ϵ represents control action at high frequencies, and τ represents the response time of the actuator command.

Table 2.23 below shows the various parameters for the actuator weighting function for each actuator command used both for simulation as well as experimental setup.

u_i	Implementation in Simulation			Implementation in Engine Test Cell		
	τ	N	ϵ	τ	N	ϵ
EGR Valve	20	3.33	0.00303	10	1	0.00303
Exhaust Throttle Valve	25	14	0.00303	25	14	0.00303
eBooster Speed	3.7	25	0.01	1	10	0.001
eBooster By-Pass Valve	30	1	0.0091	30	1	0.0091
Fueling	2	1	3.3e-05	4	1	3.3e-05

Table 3.3 Actuator Weighting Functions

The controller configuration along with the nominal plant and its associated uncertainty can be seen in figure 3.4. The controller is designed to track AFR, DAR, and engine speed with the help of the electrified air handling system for the 4.5L engine.

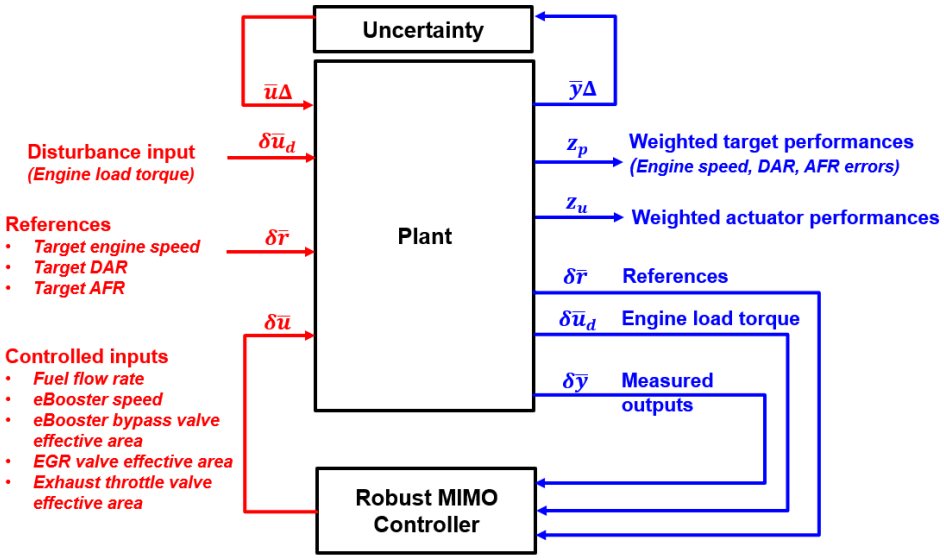

Figure 3.4. Controller Configuration for the robust MIMO controller

3.5. Results and Discussion

This section discusses results (both simulation and experimental) and comparison of engine responses for the three configurations.

1. Non eBoosted Case: This consists of the baseline 4.5L diesel engine running with the stock engine control module (ECM) without an electrified air handling system. In this case, the decoupled PID controllers are implemented to track DAR, AFR and engine speed via EGR valve, exhaust throttle valve and fueling command respectively.
2. SISO eBoosted Case: In this configuration, the 4.5L diesel engine is equipped with the baseline ECM and an electrified eBooster, which supplies additional fresh air into the cylinders during transient conditions. Additionally, a bypass valve is incorporated in parallel with the eBooster to enable fresh air intake when the eBooster is deactivated.
3. MIMO eBoosted Case: This configuration features the electrified 4.5L diesel engine with a robust MIMO controller maintaining the air handling system. The MIMO controller ensures precise tracking of DAR, AFR, and engine speed by utilizing multiple actuators, including the EGR valve, exhaust throttle valve, eBooster speed, eBooster bypass, and fueling.

3.5.1. Simulation Results

The three outlined setups are simulated within a co-simulation framework that employs both Simulink and GT-Power. Within this arrangement, the robust single-input single-output (SISO) and multiple-input multiple-output (MIMO) controllers are configured within Simulink, while the benchmark controllers and the engine model (plant) are established within GT-Power. During simulation, load torque is applied at 1800 rpm and 1600 rpm approximately 8 seconds into the simulation, transitioning from 100Nm to 500Nm at a rate of 1200Nm/s.

Figure 3.5 depicts the outcomes of implementing the controller at 1800 rpm. Given that the plant model's equilibrium was set at 1800 rpm and 300 Nm, the MIMO controller is anticipated to demonstrate sufficient robustness in managing the load transient at this speed. The left-side subplots exhibit reference tracking for Diluent Air Ratio (DAR), Air Fuel Ratio (AFR), and engine speed. Meanwhile, on the right, five subplots illustrate the actuator commands utilized by the controllers to track the desired variables. As the load ramps up, the engine speed decreases, prompting the fueling controllers to respond by increasing fueling during the transient operation. Among the three configurations, the robust MIMO controller shows the most effective engine speed recovery, with a 43% lower engine speed droop and a 65% faster recovery time compared to the non-eBoosted case. The SISO eBoosted case demonstrates better recovery than the non-eBoosted case but still lags behind the MIMO eBoosted case. In terms of Air Fuel Ratio (AFR) recovery, the MIMO eBoosted case surpasses the other configurations, with AFR dropping to approximately 18.24, whereas the SISO eBoosted and non-eBoosted cases show AFR drops to 17.79 and 16.26, respectively. The MIMO controller also exhibits a similar trend in Diluent Air Ratio (DAR) recovery. During transients, the EGR valve reduces DAR, which then returns to normal once the engine reaches a steady state after the load transient. Additionally, the exhaust throttle area remains relatively open for the MIMO eBoosted case compared to the other cases.

Figure 3.6 presents the results for SISO and MIMO controller implementation at 1600 rpm, with a similar load transient applied to the engine across all three configurations. The choice of 1600 rpm aims to showcase the controller’s robustness and stability at operating points away from the equilibrium point. The MIMO eBoosted case outperforms the other configurations, demonstrating a 47% lower droop in engine speed and a 72% shorter recovery time to return the engine speed to 1600 rpm. However, it's noteworthy that there is an overshoot in engine speed, causing it to reach steady state at approximately the same time as the other cases. This observation confirms that while the MIMO controller remains stable, its performance at 1600 rpm is not as optimal as it is at 1800 rpm.

Furthermore, the MIMO controller showcases faster recovery in Diluent Air Ratio (DAR) and Air Fuel Ratio (AFR) compared to the SISO eBoosted and non-eBoosted cases. During the MIMO eBoosted case at 1600 rpm,

the exhaust valve remains relatively open. This behavior primarily results from the measured engine AFR being lower than the desired AFR, prompting the MIMO controller to adjust accordingly.

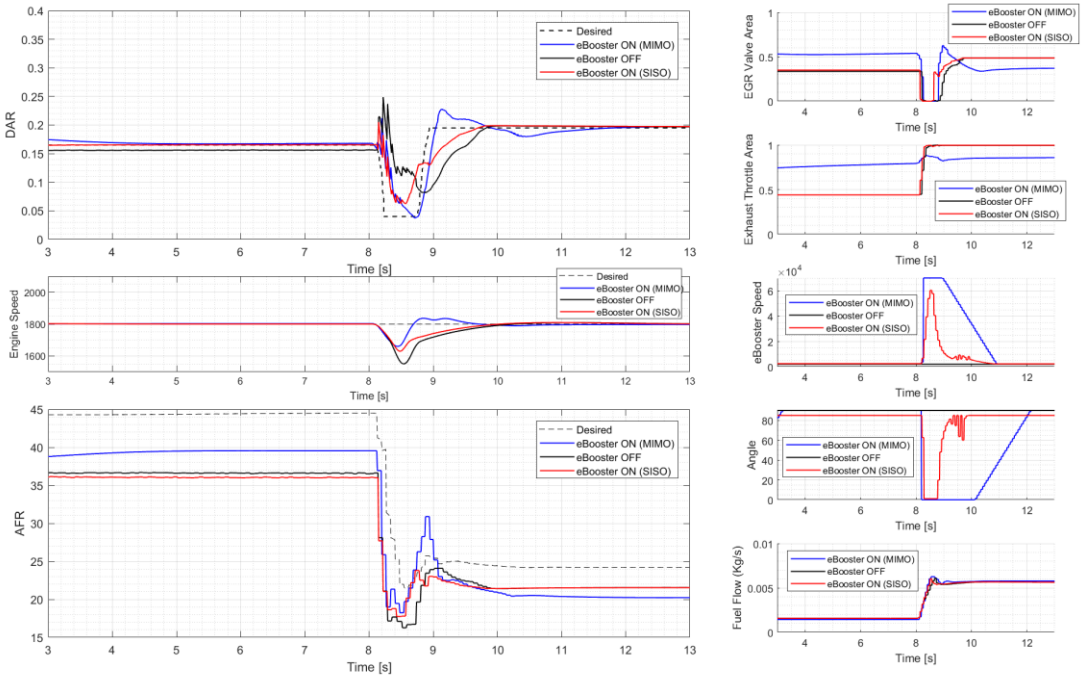

Figure 3.5. MIMO Implementation at 1800 rpm [100 Nm to 500 Nm at 1200 Nm/s]

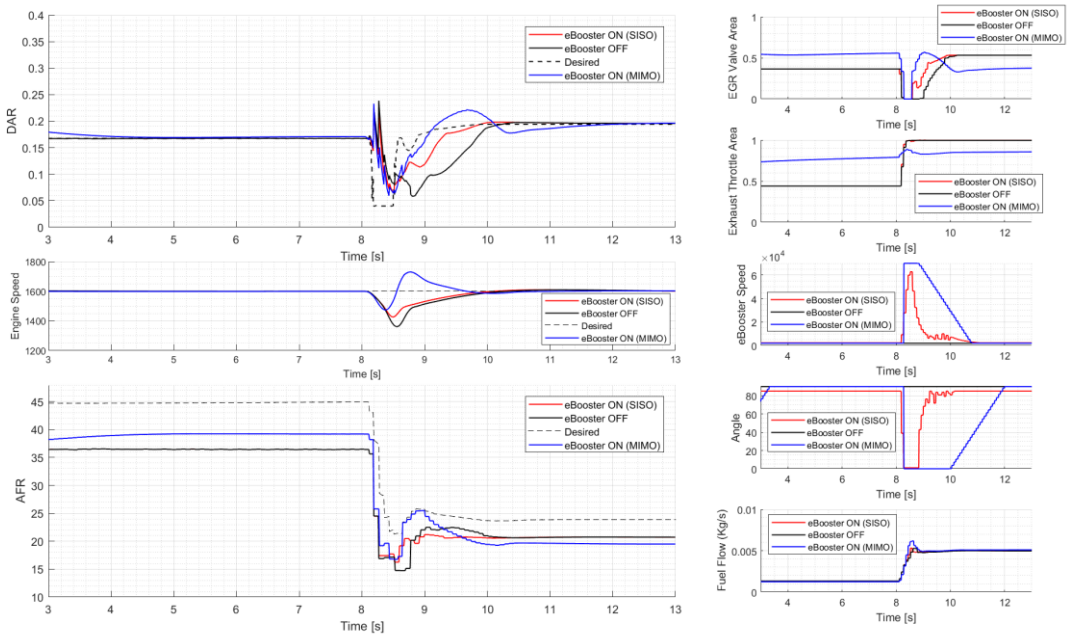

Figure 3.6. MIMO Implementation at 1600 rpm [100 Nm to 500 Nm at 1200 Nm/s]

3.5.2. Experimental Results

The SISO and MIMO controllers undergo implementation and experimental validation within the engine test cell at the University of Wisconsin. This process involves configuring the controller architectures in Simulink and then deploying them onto the engine using a dependable in-vehicle prototyping system (AutoBox) via dSPACE. The controller matrices and architectures are seamlessly integrated into the AutoBox system, facilitating communication with the baseline engine control module (ECM) and effectively superseding the actuator commands sent to the engine. To apply the load transient, an engine dynamometer coupled to the 4.5L diesel engine is utilized, ensuring a controlled and reproducible environment for the tests. Data from the test cell is captured using a high-speed data acquisition system, which is subsequently employed to generate comparison plots for the three configurations.

Figure 3.7 illustrates the results of implementing both SISO and MIMO controllers on the engine operating at 1800 rpm, alongside comparisons with other configurations. A load step ranging from 100Nm to 500Nm was applied at a rate of 1200 Nm/s. The experimental findings demonstrate the successful implementation of both SISO and MIMO controllers, clearly showcasing the superiority of the MIMO controller over the other configurations.

The MIMO eBoosted case showcases a notable 45% reduction in engine speed droop compared to the non-eBoosted case, with its recovery time impressively shortened by 70%. Furthermore, it displays superior recovery in both Diluent Air Ratio (DAR) and Air Fuel Ratio (AFR) during transient operations. The EGR valve closes during load transients to match the desired DAR, reopening when the engine speed returns to 1800 rpm. To maintain the desired AFR, the exhaust throttle valve is partially open at low loads. This throttling of air at low loads assists in heating the exhaust gas entering the aftertreatment system, aiding in the passive regeneration of the Diesel Particulate Filter (DPF).

During low-load conditions, less fueling is necessary to maintain engine speed, enabling the partial closure of the exhaust throttle while still achieving an appropriate AFR and effectively heating up the exhaust gas. The eBooster is activated solely during the load transient and promptly deactivated once the engine reaches a steady state. Additionally, the bypass valve closes during the transient to fully utilize the capabilities of the eBooster. The fueling from the MIMO controller reacts faster to the drop in engine speed than the other cases, thereby aiding in improving the speed response.

Figure 3.8 presents the experimental results for SISO and MIMO implementation at 1600 rpm, with a similar load transient ranging from 100 Nm to 500 Nm applied at 1200 Nm/s. The choice of 1600 rpm helps demonstrate the robustness of the MIMO controller in performing at an operating point away from the equilibrium range. At 1600 rpm, the MIMO controller emerges as the superior configuration. It exhibits a remarkable 55% reduction in engine speed droop, along with a 69% shorter recovery time compared to the non eBoosted case. Although the droop in engine speed for the SISO eBoosted case matches that of the MIMO eBoosted case, the SISO eBoosted case takes roughly twice as much time to recover.

In summary, both the MIMO and SISO controllers are effectively implemented and experimentally verified on the engine, underscoring the benefits of employing an electrified compressor during transient load operations. The experimental findings from the engine test cell align closely with the results obtained from simulations. The decoupled SISO system for the eBooster is found to be suboptimal due to its limited understanding of other actuators that can impact the air handling system. Leveraging the knowledge of interconnections among various actuator inputs and model outputs, the MIMO controller emerges as the most efficient solution for the engine's air handling system, enhancing the engine's capability to handle transient operations through the integration of an electrified compressor.

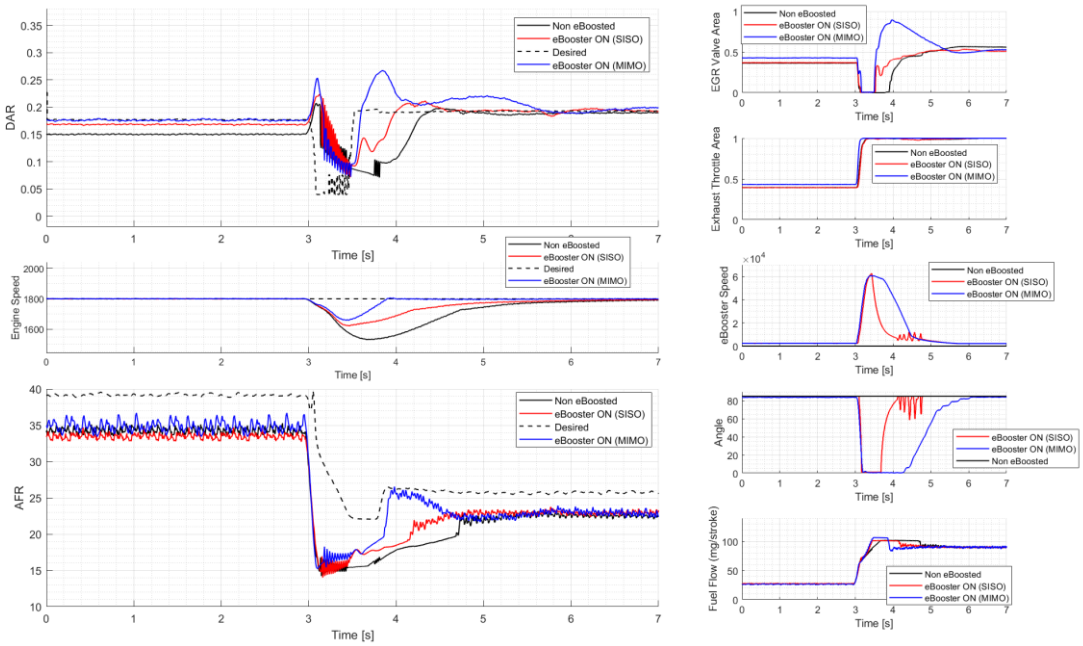

Figure 3.7. MIMO Implementation at 1800 rpm [100 Nm to 500 Nm at 1200 Nm/s]

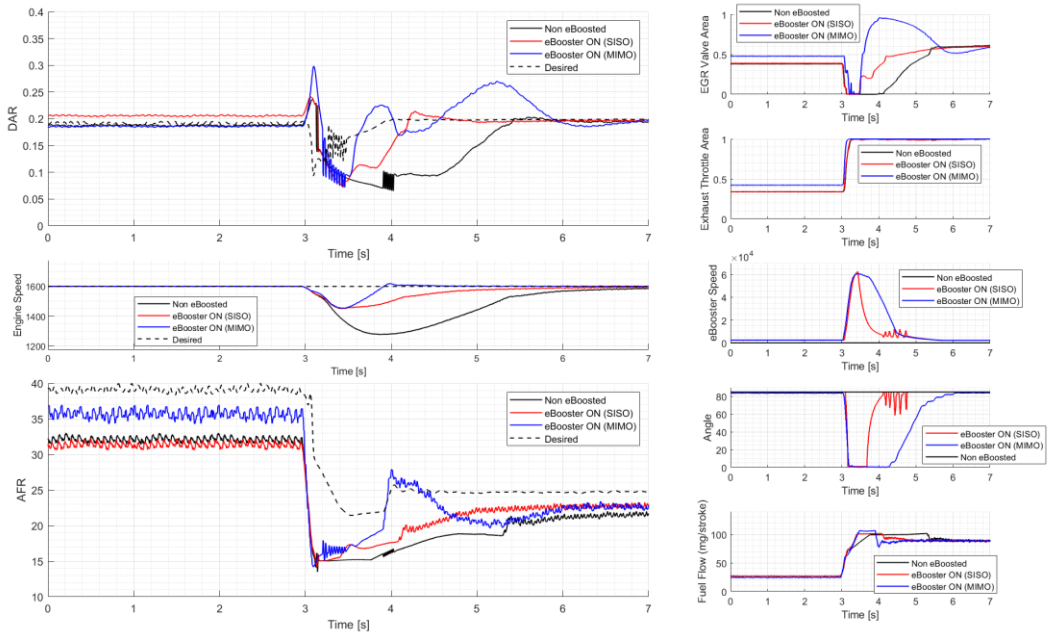

Figure 3.8. MIMO Implementation at 1800 rpm [100 Nm to 500 Nm at 1200 Nm/s]

4. CONCLUSIONS

This paper discusses the benefits of developing robust coordinated control strategies for a highly non linear air handling system over the conventional decoupled controllers that we see in today's industry. Overall, both the MIMO and SISO controllers were successfully implemented and experimentally tested on the 4.5L diesel engine. The experimental results obtained from the engine test cell align well with the simulation outcomes. The results for the implementation of the SISO eBooster controller demonstrates the benefits of deploying an electrified air handling system to improve the engine performance for load transient operation. By utilizing the knowledge of coupling between various actuator inputs and model outputs, the MIMO controller proves to be the most effective for the engine's air handling system, enhancing the engine's load acceptance during transient operations through the use of an electrified compressor.

5. REFERENCES

[1] Dallmann, T., & Menon, A. (2016). Technology pathways for diesel engines used in non-road vehicles and equipment. *International Council on Clean Transportation (ICCT): Washington, DC, USA*.

[2] Kean, A. J., Sawyer, R. F., & Harley, R. A. (2000). A fuel-based assessment of off-road diesel engine emissions. *Journal of the Air & Waste Management Association*, *50*(11), 1929-1939.

[3] Ecker, H. J., Schwaderlapp, M., & Gill, D. K. (2000). *Downsizing of diesel engines: 3-cylinder/4-cylinder* (No. 2000-01-0990). SAE Technical Paper.

[4] Ricardo, M. B., Apostolos, P., & Yang, M. (2011). Overview of boosting options for future downsized engines. *Science China Technological Sciences*, *54*, 318-331.

[5] Alshammari, M., Alshammari, F., & Pesyridis, A. (2019). Electric boosting and energy recovery systems for engine downsizing. *Energies*, *12*(24), 4636.

[6] Kiwan, R., Middleton, R., & Stefanopoulou, A. (2018). *Thermodynamic and practical benefits of waste energy recovery using an electric turbo-generator under different boosting methods* (No. 2018-01-0851). SAE Technical Paper.

[7] Nazari, S., Siegel, J., & Stefanopoulou, A. (2019). Optimal energy management for a mild hybrid vehicle with electric and hybrid engine boosting systems. *IEEE Transactions on Vehicular Technology*, *68*(4), 3386-3399.

[8] Zhao, D., Stobart, R., Dong, G., & Winward, E. (2014). Real-time energy management for diesel heavy duty hybrid electric vehicles. *IEEE Transactions on Control Systems Technology*, *23*(3), 829-841.

[9] Nazari, S., Stefanopoulou, A., Kiwan, R., & Tsourapas, V. (2016, October). A coordinated boost control in a twincharged spark ignition engine with high external dilution. In *Dynamic Systems and Control Conference* (Vol. 50701, p. V002T20A003). American Society of Mechanical Engineers.

[10] Nazari, S., Siegel, J., & Stefanopoulou, A. (2021). Control of hybrid boosting in highly diluted internal combustion engines. *International Journal of Engine Research*, *22*(6), 1794-1807.

[11] Xiao, B., Buckland, J. H., & Karnik, A. (2017, October). Frequency separation control of series sequential boosting system with electric supercharger and turbocharger. In *Dynamic Systems and Control Conference* (Vol. 58295, p. V003T34A004). American Society of Mechanical Engineers.

[12] Ekberg, K., & Eriksson, L. (2017). Improving fuel economy and acceleration by electric turbocharger control for heavy duty long haulage. *IFAC-PapersOnLine*, *50*(1), 11052-11057.

[13] Villegas, J., Gao, B., Svancara, K., Thornton, W., & Parra, J. (2011, September). Real-time simulation and control of an electric supercharger for engine downsizing. In *2011 IEEE Vehicle Power and Propulsion Conference* (pp. 1-6). IEEE.

[14] Bristol, E. (1966). On a new measure of interaction for multivariable process control. *IEEE transactions on automatic control*, *11*(1), 133-134.

[15] Harsha Rayasam, S., Qiu, W., Rimstidt, T., Shaver, G. M., Van Alstine, D. G., & Graziano, M. (2023). Control-oriented modeling, validation, and interaction analysis of turbocharged lean-burn natural gas variable speed engine. *International Journal of Engine Research*, *24*(2), 738-754.

[16] Qiu, W., Rayasam, S. H., Shaver, G. M., Rimstidt, T. G., & Van Alstine, D. G. (2023). Control design-oriented modeling and μ-synthesis-based robust multivariate control of a turbocharged natural gas genset engine. *International Journal of Engine Research*, *24*(9), 3905-3921.

[17] Rayasam, S. H., Qiu, W., Rimstidt, T., Shaver, G. M., & Van Alstine, D. G. (2023). Robust model-based switching MIMO air handling control of turbocharged lean-burn SI natural gas variable speed engines. *International Journal of Engine Research*, *24*(6), 2783-2804.

[18] Qiu, W., Rayasam, S. H., Shaver, G. M., Rimstidt, T., Van Alstine, D. G., & Graziano, M. (2022). Modeling and Robust Coordinated Control of Turbocharged Natural Gas Engine with Genset Application. *IFAC-PapersOnLine*, *55*(24), 39-44.

[19] Rayasam, S. H., Qiu, W., Shaver, G. M., Rimstidt, T., & Van Alstine, D. G. (2022). Robust Switching MIMO Control of Turbocharged Lean-Burn Natural Gas Engines. *IFAC-PapersOnLine*, *55*(24), 7-12.

[20] Qiu, W. (2023). AN INTEGRATED FRAMEWORK FOR MODELING, ROBUST COORDINATED CONTROL, AND POWER MANAGEMENT OF ADVANCED POWERTRAINS FEATURING TURBOCHARGED ENGINES (Doctoral dissertation, Purdue University Graduate School).

[21] Chen, Z., Chen, Z., & Yao, B. (2021). Modeling and H∞ position control of a spreader in the gantry crane. IFAC-PapersOnLine, 54(20), 592-597.

[22] Qiu, W., Ashta, S., Shaver, G. M., Mazanec, J., Kokjohn, S., Johnson, S. C., ... & Frushour, B. C. (2024). System configuration, control development, and in-field validation of a hybrid electric wheel loader featuring electrically-boosted engine. Control Engineering Practice, 150, 105989.